PROCEEDINGS, 46th Workshop on Geothermal Reservoir Engineering
Stanford University, Stanford, California, February 15-17, 2021
SGP-TR-218

Study on Foam Fracturing of Granite for the Development of Enhanced Geothermal Systems[a]

Hong Wang[1,*], Jy-An J. Wang[1], Yarom Polsky[2], Fei Ren[3], Viren Thakore[3]

[1]Materials Science & Technology Division, Oak Ridge National Laboratory, PO Box 2008, MS 6069, Oak Ridge, TN 37831

[2]Electrification & Energy Infrastructure Division, Oak Ridge National Laboratory, PO Box 2008, MS 6075, Oak Ridge, TN 37831

[3]Temple University, 1947 North 12th Street, Philadelphia, PA 19122

*Corresponding Author. E-mail: wangh@ornl.gov

Keywords: foam fracturing, granite, cyclic injection, waterless, EGS stimulation

ABSTRACT

Foam fracturing has been considered as a potential approach to address water utilization concerns with hydraulic stimulation in the development of enhanced geothermal systems (EGS). This paper reports the recent progress of a project sponsored by the U.S. DOE's Geothermal Technologies Office (GTO) Waterless Stimulation Initiative. The objective of project is to assess the feasibility of foam fracturing as an alternative approach to hydraulic fracturing. This paper describes the development of a foam fracturing test system at Oak Ridge National Laboratory (ORNL), which can be used to perform hydraulic fracturing of rock-like materials with both water and foamed liquids under pressure to 6,000 psi (41.4 MPa). The system, which consists of two sections: one for foam generation and the other for foam injection, has the capability of testing materials under pressure control in both monotonic and cyclic (up to 50 Hz) injection modes.

Experimental results of foam fracturing on Charcoal Black granite are reported for cylindrical specimens with a blind hole studied using water and nitrogen-gas-in-water foam as the fracturing fluids. The effects of fracturing fluids and injection modes on the breakdown pressure and failure responses of the material were examined. The observations from the experimental work and the implications to EGS application are presented and discussed.

1. INTRODUCTION

Foam fracturing is considered a potential approach to address water availability challenges with development of enhanced geothermal systems (EGS). Currently, EGS relies on water for hydraulic stimulation to create the fracture network required for extraction of geothermal energy. One study of the use of water in geothermal plant development estimated that nearly 2 million gallons (7,570 m^3) per MW are required for EGS reservoir stimulation (Clark et al. 2011). To achieve the U.S. DOE goal of 60 GW of geothermal power generation capacity by the year 2050 (U.S. DOE, 2019), approximately 120 billion gallons (454 million m^3) of water would be needed for hydraulic stimulation if alternatives to hydraulic stimulation are not developed. This does not consider water needs for well construction such as drilling and cementing. The challenge of meeting resource needs for EGS well construction and completion is further compounded by the fact that the majority of the most promising potential EGS sources in the U.S. are located in the regions where water stress is high or extremely high (Blackwell et al., 2011; Freyman, 2014). Therefore, technology innovation is needed to overcome technical and non-technical barriers and to mitigate the upfront cost and risk with reservoir stimulation. This study focuses on assessing the feasibility of foam fracturing to overcome these barriers as part of the U.S. DOE waterless stimulation initiative.

Foam is an immiscible mixture of liquid and gaseous phases that behaves quite differently from the single constituent phases. For example, the viscosity of foam can be many times that of single phases like water or gas, depending on the quality of foam (gas volumetric fraction in mixture). The tunable properties of foam have been shown to be extremely attractive to EGS reservoir engineering. The high viscosity can reduce fluid leakage, increase fracture width, and improve proppant transportation, while it is compressible with high energy storage capabilities, providing sustained driving force for fracture propagation. Additionally, the gas has very high permeability to penetrate the stressed body to create more complete fractures. Generally, an optimal foam performance can be obtained when the quality is 70% or higher (Faroughi et al., 2018). The implication is that a substantial amount of water can be replaced by the gaseous phase and, therefore, the usage of water can be reduced accordingly.

Foam fracturing has been used on a very limited basis in oil and gas fields dating back to the 1970's, primarily in low pressure and low permeability formations, but continues to be a subject of research investigation with additional technical challenges related to EGS implementation. EGS reservoir conditions and lithologies are substantially different from those of oil and gas. The earth stresses and temperature are generally higher and prospective EGS reservoirs are typically composed of rocks such as granite, which has higher strength and orders of magnitude less permeability than the typical sedimentary rocks in deep conventional oil and gas reservoirs. The

stability and stimulation effectiveness of foam fluids for these conditions is an open question along with additional concerns related to mitigation of induced seismicity. We propose to evaluate the stability and effectiveness of foamed fluids for EGS scenarios and use pulsed or cyclic injection to address these challenges. This is a new concept with many potential advantages including more efficient and reduced water usage and improved control of reservoir seismicity. Some research considerations and preliminary work using model material have been reported previously (Wang et al., 2019; 2020). In this paper, ORNL's foam fracturing testing system is introduced. The system has a capability of conducting foam fracturing in both monotonic and cyclic pressure injection modes with a pressure rating of 6,000 psi (41.4 MPa). Then, experimental results for granite are presented. The granite specimens tested were cylinders with a blind hole. The fracturing fluid was foamed with nitrogen gas with quality higher than 70% using alfa olefin sulfonate (AOS) as a surfactant. In monotonic injection, the breakdown pressure of granite specimens under foam fracturing tended to increase, but it was not statistically significant. On the other hand, we have observed the breakdown pressure can be brought down to 70% of the monotonic breakdown pressure by using low cycle fatigue. Finally, discussions are presented regarding injectivity and water use reduction.

2. EXPERIMENTAL TECHNIQUE

2.1 Foam Fracturing Test System

A schematic of the system is shown in Fig. 1 (a). It consists of individual liquid and gas phase sections, foam generation and foam injection. The critical components for gas and liquid sections, foam generation and foam injection are shown in Fig. 1 (b-d).

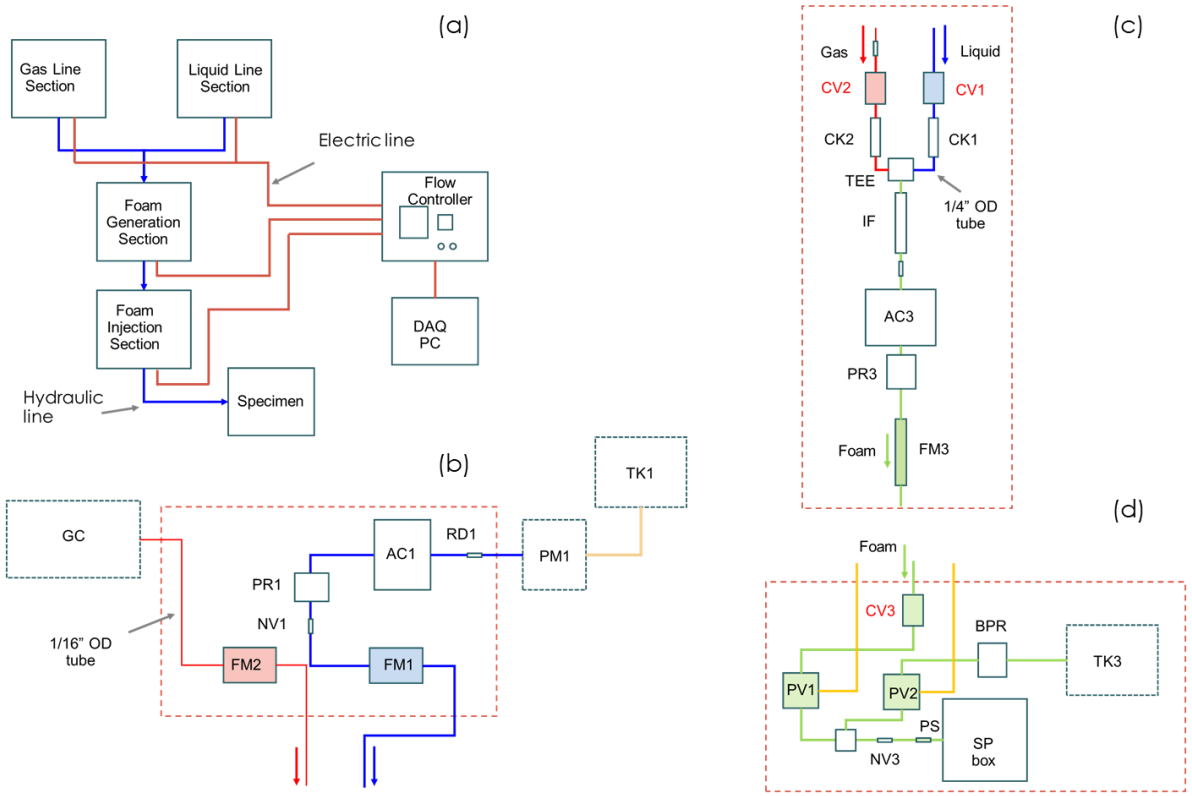

Figure 1: (a) Schematic of foam testing system, (b) liquid and gas sections, (c) foam generation section, and (d) foam injection section, where GC- gas cylinder, TK- tank, PM- pump, AC- accumulator, PR – pressure regulator, RD – rupture disk, NV – needle valve, FM – (mass) flow meter, CV – control valve, CK – check valve, IF – inline filter, PV – pulsed valve, BPR – back pressure regulator, PS – pressure sensor, SP – specimen; suffixes 1, 2 and 3 refer to either liquid, gas, foam or dual valves in PV, respectively.

Foam is produced by mixing pressurized liquid and gas phases in a pre-determined volumetric ratio. In the liquid line, a solution is pressurized using an air-driven pump (PM1) that has a maximum outlet pressure of 8,875 psi (61.2 MPa). A 1-gallon bladder accumulator (AC1) is used to attenuate the pressure fluctuation and to store the liquid for subsequent operation. A pressure regulator (PR1) is used to set the pressure level with the help of a needle valve (NV1). Thereafter, an electric control valve (CV1) is used to control the flow rate of the liquid line with the input from thermal mass flow meter (FM1). In parallel to the gas line, a second electric control valve (CV2) is used to control the flow rate of gas with the input from another thermal mass flow meter (FM2). The pressurized gas is supplied by a 6,000- psi (41.4 MPa) gas cylinder. The pressure level and flow rate are also preset by the pressure regulator and needle valve installed. Both lines have a check valve (CV1 or CV2) to prevent backflow before they mix at the tee connector. The foam mixture is homogenized by passing through an in-line filter (IF) before being stored in another bladder accumulator (AC3). The pressure and flow rate in the foam line are preset with pressure regulator PR3 and back pressure regulator BPR; the foam flow rate is controlled by an electric control valve (CV3) with the input from a Coriolis mass flow meter (FM3). The CV1, CV2, and CV3 are operated using a WATLOW controller. In

foam injection mode, a dual valve system (PV1 and PV2) is used to apply a pressure pulse to the specimen under test (SP). PV1 and PV2 are electrically controlled, pneumatically driven valves. The dual valves are controlled by a timer to cycle pressure for pulsed fracturing experiments. The WATLOW controller and the timer for PVs are mounted in a control panel.

Pressure gauges are installed next to the pressure sources to monitor the outlet pressures including pump, gas cylinder, pressure regulators. A pressure sensor is installed ahead of the specimen to measure the pressure applied. The signals from the pressure sensor and the mass flow meters are acquired using a MC USB-230 series device. The foam density signal measured by FM3 was acquired by a Bronkhorst FlowPlot. A client server, FlowDDE, needs to be started to run the FlowPlot. A video camera was used to record the fracturing process. The video data were processed and synchronized with the signals from the data acquisition offline.

316 stainless steel (SS) tubes with 1/16" (1.59 mm) and ¼" (6.35 mm) outside diameters (OD) are used in the gas and liquid/foam lines, respectively. All the devices, tubes and fittings are rated with pressure at least 6 000 psi (41.4 MPa).

A typical test generally consists of two steps: foam generation and foam injection. The former begins with setting up gas and liquid line pressure and mass flow rate. The process then uses PR3 and BPR to maintain a specific foam mass flow rate set point while adjusting CV1, CV2 and, if necessary, CV3 to achieve a target foam density. The adjustment of CVs is done manually on the controller. After the target foam density has been obtained, foam is injected into the test sample. In the case of monotonic injection, the pressurization is applied through manually turning the PR3. For the cyclic injection, a timer is used to automate the process. In this study, a 4-sec period was used in cyclic injection defined by a 2-sec pulse length and a 2-sec pulse delay, equivalent to 50% duty cycle. The pressure is oscillated between high- and low- pressure values. A flow chart is shown in Fig. 2 for the procedures discussed.

Cyclic stimulation has been used in EGS field development before (Zimmermann et al., 2010; Chabora and Zemach, 2013). These previous efforts controlled pumping operations at the surface with pressure cycling accomplished by intermittent fluid injection over periods of hours or days. The approach in this study is quite different in that high frequency pressure cycling is explored without cessation of pumping (i.e. pressure is cycled between a high- and low- pressure value). This functionality is accomplished by the active control of flow valves and enables controlled exploration of the potential for stimulating rock failure by fatigue.

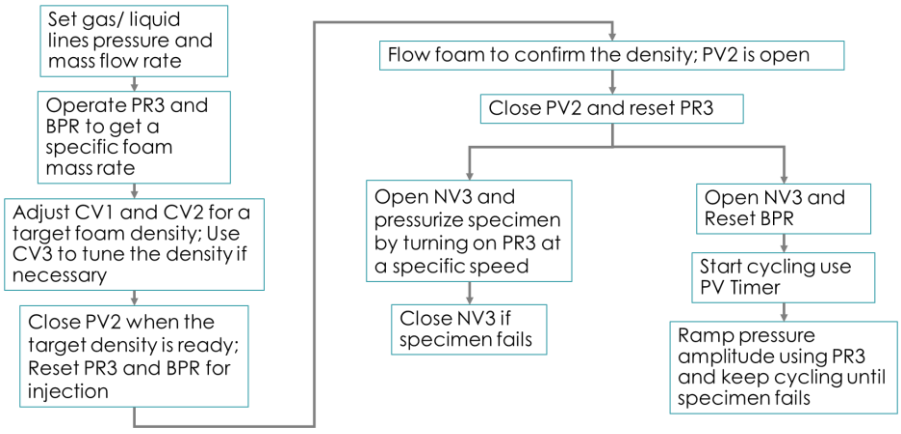

Figure 2: Flowchart of testing procedures; CV1, CV2, and CV3 are control valves for liquid, gas and foam; PR3 is pressure regulator for foam; PV2 is pulsed valve in discharge line; NV3 is needle valve for specimen; BPR is back pressure regulator.

2.2 Test Materials

Granite is one type of the source rocks widely seen in EGS sites around the world (Xie et al., 2015) and it was examined. Charcoal Black granite used in this study was supplied by Coldspring (Cold Spring, MN). This material was studied previously (Lu et al., 2015). The modulus of rupture is 16.7 MPa (based on ASTM C99 as supplied by the supplier). The longitudinal wave velocity was measured to be 4,082 ± 111 m/s for a representative set of samples, and the shear wave velocity was measured to be 2,711 ± 91 m/s. Granite specimens were cylinders sized with 50.80 mm in diameter, and 101.60 mm in length. All samples were internally pressurized through a blind 9.53 mm borehole drilled to the axial mid-point of the specimen. The blind hole specimen was used in this study because the configuration resembles the stimulation condition at the end of a borehole in the field (Li et al., 2015; Wanniarachchi et al., 2018).

A 316 SS 6.35 mm OD × 4.57 mm ID tube served as a fluid conduit to the borehole. The OD of the tube was bonded to the hole surface using 3M high-strength epoxy DP420 (St. Paul, MN) and allowed to cure for at least 24 hours before testing to achieve full mechanical strength. Epoxy was not applied to the lower 6.35 mm of the tube, which was used as part of the pressurizing zone. The tube was also extended about 44.45 mm outside of the specimen for pressure fitting connection. Two O-rings were installed to prevent the epoxy from flowing to the bottom of the blind hole. The length of bonding was selected to withstand pullout of the tube at a specified pressure level. The same configuration of specimen – tube assembly was used in the study of cement foam fracturing (Wang et al., 2020). Experimental results for total 20 specimens are reported including 10 each for monotonic injection and cyclic injection. In each injection mode, 5 were subjected to water fracturing and 5 were subjected to foam fracturing.

2.3 Foam

A range of candidate foams were studied for potential use in waterless stimulation of EGS. For this study, the primary candidates of interest were N_2-based foams. The N_2 was used in this stage also because the required pressurized gas can be provided by a commercial high-pressure gas cylinder, which simplifies the test setup. Experimental fracture testing to date has used N_2 as a gaseous phase at 70% or higher quality with 1 wt.% AOS as a surfactant. The relevant properties of the foam can be found in Thakore et al. (2020; 2021).

2.4 Data Processing and Analysis

The mass for each phase was obtained through the integral of mass (flow) rate or

$$M_i = \int \dot{M}_i \, dt, \tag{1}$$

where M is mass in gram and $\dot{M}$ the mass rate output from flow meters, g/min; subscript i = f, g, w, each representing foam, gas, and water, respectively; same comment applied in the following. The mass flow meter, calibrated by the factory, was also verified in the lab by using the mass collected at a specified time. The foam quality (Γ), defined as a ratio of gas volume to foam volume (gas + liquid), can be expressed by

$$\Gamma = \frac{\rho_w - \rho_f}{\rho_w - \rho_g}, \tag{2}$$

where subscripts w, g and f have same meaning as before. ρ_g= 1000 kg/m^3 and ρ_f is measured by the Coriolis mass flow meter. The gas density, ρ_g, is estimated according to

$$\rho_{g2} = \frac{P_2}{T_2}\frac{T_1}{P_1}\rho_{g1}, \tag{3}$$

where ρ is density in kg/m^3; T temperature in ^{o}C; subscripts 1 and 2 represent gas conditions; P pressure in MPa, measured by the pressure sensor (Valvias, 2020). Because our tests were carried out at room temperature, thus we have T_1= T_2; the two items thus cancelled out in Eq. (3). In this study, conditions 1 and 2 refer to ambient and pressurized conditions, respectively. At the ambient condition, P_1 = 14.5 psi (0.1 MPa), N_2 density ρ_{g1} = 1.25 kg/m^3. Once the gas pressure is given, the gas density under pressurized condition can be calculated. The gas mass rate, $\dot{M}_g$, can be estimated according to

$$\dot{M}_g = \Gamma\frac{\rho_g}{\rho_f}\dot{M}_f, \tag{4}$$

and water mass rate, $\dot{M}_g$, can be obtained using mass equilibrium by

$$\dot{M}_w = \dot{M}_f - \dot{M}_g. \tag{5}$$

Injectivity index, *II*, for each phase can be calculated by

$$II_i = \frac{\dot{M}_i}{P}, \tag{6}$$

where *II* is in g/(min*MPa), subscript i = f, g, w. Furthermore, mass ratio (MR, ξ) and mass rate ratio (MRR, η) are defined to characterize the extent of water reduction or replacement,

$$\xi_i = \frac{M_i}{M_f}, \tag{7}$$

$$\eta_i = \frac{\dot{M}_i}{\dot{M}_f}, \tag{8}$$

where subscript i = g, w.

3. EXPERIMENTAL RESULTS

3.1 Monotonic Injection

A typical set of pressure and mass flow rate curves is shown in Fig. 3 along with the snapshots from video camera for water fracturing tests performed on a specimen labeled g2019. The fracture initiation and specimen breakdown can be identified and verified with obtained data. On the pressure curve, the pressurization rate decreased upon fracture initiation and peaked at breakdown. Mass flow rate displayed a sharp spike initially followed by a gradual decline. Near peak pressure, mass flow rate exhibited a rapid increase signifying fracture initiation and a second spike upon specimen failure. The fracture initiation and breakdown were validated by the images showing water leaks and water eruption. These images illustrate that, after fracture initiation, the cracks grew and coalesced first longitudinally on the top, and then transversely, resulting in the final breakdown.

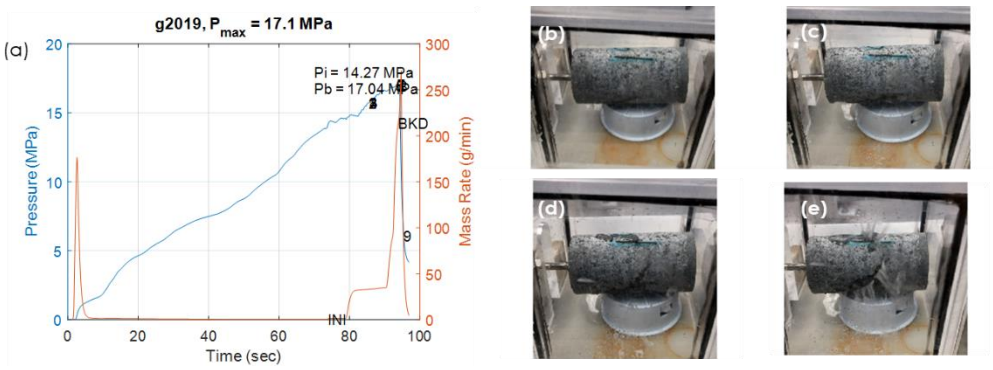

Figure 3: Monitoring-based responses for g2019, water as a fracturing fluid: pressure & mass rate; video-based process for g2019 for (b) event 1: 85.37s, water leak in bottom; (c) 5: 93.23s transverse crack coalescence on top; (d) 8: 94.22s transverse crack coalescence extended; (e) 9: 95.38s large water overflow. INI – fracture initiation, BKD – breakdown.

The foam fracturing responses are shown in Fig. 4 with specimen g2013 as an example. The fracture initiation and specimen breakdown can be identified in a manner similar to water fracturing experiments. On the pressure curves, these events corresponded to a small step and final peak following by the rapid pressure drop. Mass flow rate tended to decline during the pressure ramp up to breakdown with several transient events occurring during fracture initiation and final breakdown. Density measurements for foam experiments were very sensitive to the mass flow rate. As a result, there was a strong response of density to the fracture initiation with a large size spike. Overall, there was a clear increasing trend in density during pressurization, mainly attributed to the increase in gas density; generally, the quality of the foam stayed quite high near 93%. The gas mass rate increased while the water mass rate decreased as expected when the pressure was increased. This is significant because it showed the replacement of water can be substantial especially at the high level of pressurization. The fracture initiation and breakdown can be validated from the snapshots. The foam fracturing features a primary longitudinal fracture with a secondary transverse fracture as can be seen from the leaking foam on the surface of specimen.

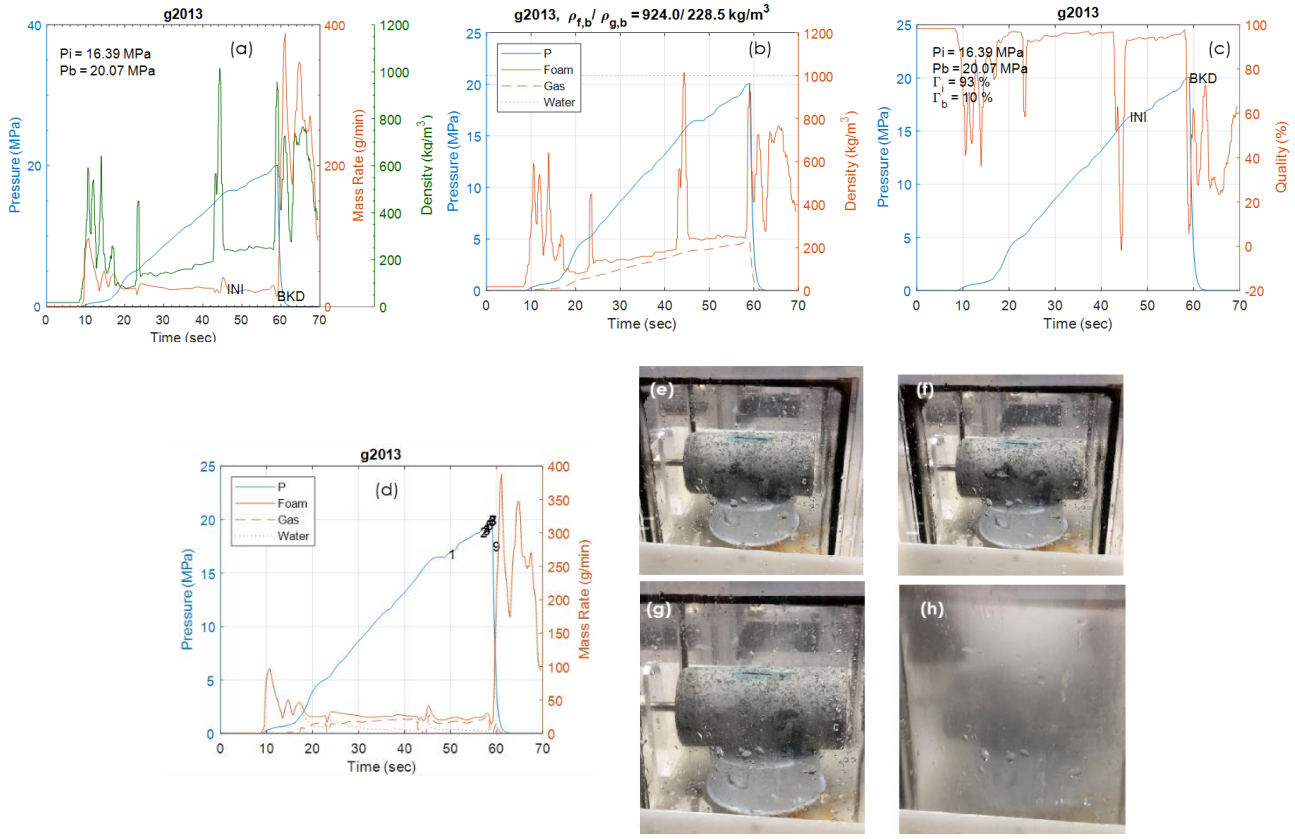

Figure 4: Monitoring-based responses for g2013, foam as a fracturing fluid: (a) pressure, mass rate and density, (b) density, (c) quality, (d) mass rate decomposed; video-based process for g2013 for (e) event 1: 49.55s, fracture initiated; (f) 2: 56.51s mixture ejection; (g) 5: 57.66s increased ejection; (h) 6: 58.26s breakup.

A summary of pressure response is shown in Fig. 5 for water fracturing and foam fracturing in terms of cumulative mass injection. The pressure curves are shown to be confined into a zone even though the pressurization times of data group varied in a wide range. All the curves feature an almost linear rise to fracture initiation and then a yielding period before the final breakdown. A small slow rise generally took place before the linear stage because of initial cavity filling of tube and specimen hole. Specimen g2022 entered directly into the linear stage because it was accidentally pressurized to 3.4 MPa before reset. Specimens g2003 and g2011 responded a little differently with a discontinuous pressure increase arising from the re-start of pump.

In general, the slope of the linear stage before the initiation, which defines the injection modulus, was higher in water fracturing than in foam fracturing. The incremental injection mass from the fracture initiation to the breakdown was greater in water fracturing than in foam fracturing. The initiation and breakdown pressures were higher in foam fracturing than in water fracturing, but the differences were relatively small (on average less than 5%). The fracture initiation pressure depends on the tensile strength and the permeability of the materials (Haimson & Fairhurst, 1969). We observed that facture initiation pressure is close to but lower than the reported modulus of rupture for the material.

The injectivity response is given in Fig. 6 for both water and foam fracturing cases. For all curves in water fracturing, the injectivity index generally fell fast into a valley and rose quickly to a plateau right after the fracture initiation. Additional plateaus were sometimes seen for some samples before breakdown. In the case of foam fracturing, a similar trend can be seen in injectivity response. Moreover, the mass increment from fracture initiation to breakdown in foam fracturing was much smaller than those in water fracturing. As a result, the injectivity index difference between the two was relatively small.

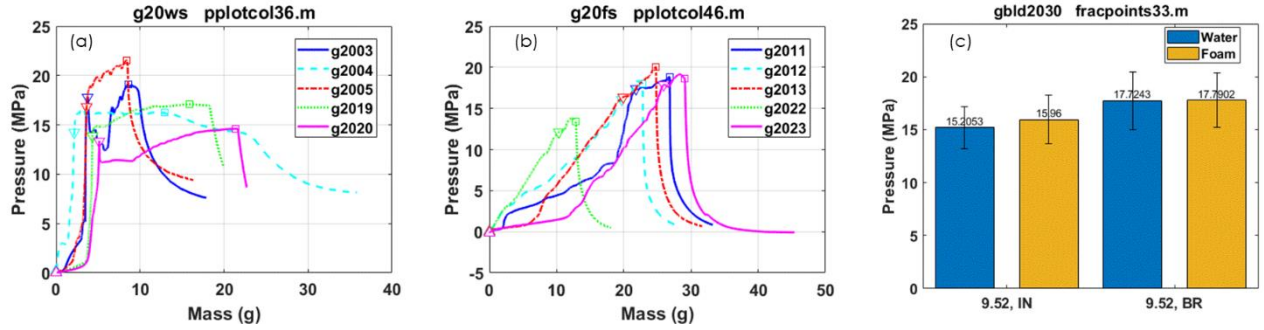

Figure 5: (a, b) Pressure as a function of injection mass for (a) water and (b) foam fracturing, (c) bar graph of fracture initiation and breakdown pressures. Upright triangle, inverted triangle and square correspond to pressurization initiation, fracture initiation and breakdown, respectively; error bar corresponds to half of standard deviation; IN – fracture initiation, BR – breakdown; same comments apply for the results presented for monotonic injection in the following.

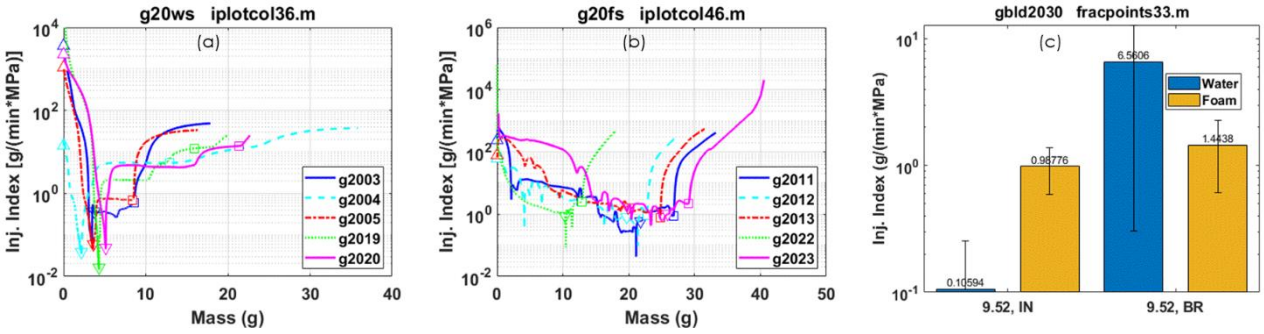

Figure 6: (a, b) Injectivity index as a function of injection mass for (a) water and (b) foam fracturing, (c) bar graph of initiation and breakdown injectivity index.

3.2 Cyclic Injection

Cyclic responses are presented in Fig. 7 with g2006 as an example in which water was used as a fracturing fluid. The pressure peak was, in general, consistent during cycling. A detailed examination revealed the peaks of pressure and mass flow rate were offset. This can be seen at points B, C for the cycle, where points A and C correspond to the states of PV1 on/ PV2 off and PV1 off/ PV2 on, respectively. Note that the control valve is a type of needle valves with regulator stem. The shape of the pressurization wave form is likely associated with the behavior of the control valve.

The maximum and minimum of injectivity index, iimax and iimin, identified for each cycle are shown in Fig. 7 (d). Both extremes exhibited a relatively steady increase before abrupt rise at the failure. The pressure peak-based injectivity index, iippk, was calculated using the pressure and mass flow rate at the pressure peak C and is presented in the same figure. The peak-based injectivity index, iippk, was observed to be more sensitive to the fatigue, and thus, will be focused in the discussion following.

The fatigue fracturing responses under cyclic injection are summarized for the tests with water as a fracturing fluid and presented in Fig. 8 in terms of maximum pressure, pmax, maximum mass rate, qmax, and peak pressure-based injectivity index, IIppk. There is not a clear relationship evident in the data between the fatigue life and maximum injection pressure. The fatigue rate, measured by the increase in injectivity index per cycle, appeared to be higher for the specimen with a shorter fatigue life. In addition, the specimen with a relatively high initial injectivity tended to have a shorter fatigue lifetime. Such initial injectivity could be related to the pre-existing structural condition and pressure ramping-induced damages before cycling.

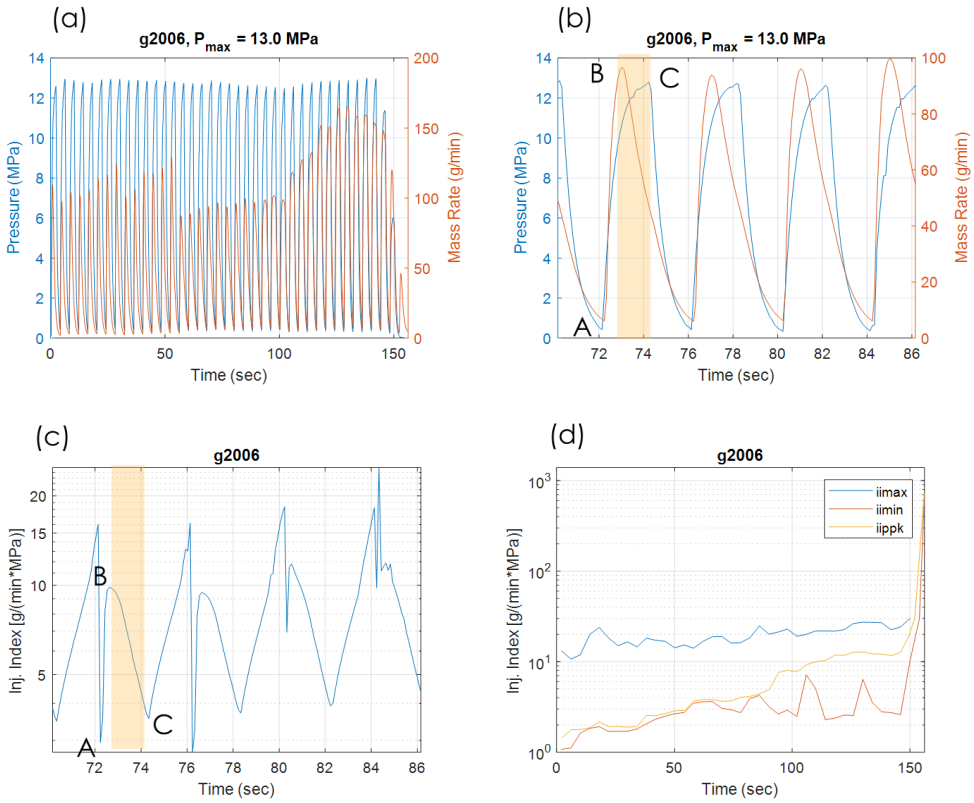

Figure 7: Waveforms of pressure and mass rate in cyclic injection of g2006 for (a) whole cycling and (b) middle life; injectivity index for (c) middle life and (d) whole cyclic process; water as fracturing fluid. Labels have the following meanings: A- PV1 on/ PV2 off; B- flow reaches peak; C- PV1 off/ PV2 on.

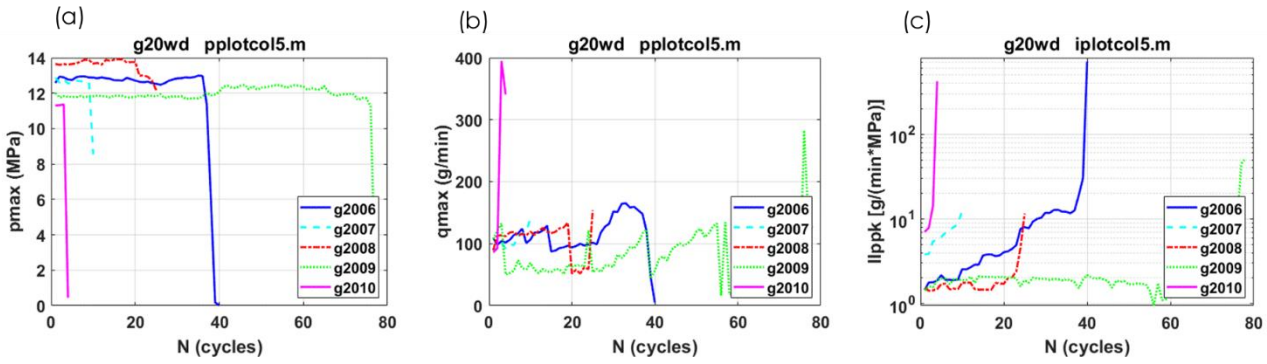

Figure 8: Cyclic injection responses for (a) maximum pressure, (b) mass flow rate and (c) injectivity index; water as a fracturing fluid.

Cyclic injection results for foam fracturing are shown in Fig. 9 with test specimen g2015 as an example. The pressure peaks were observed to be mostly consistent during the cycling process and fell to zero at the failure. Mass flow rate peak varied arbitrarily in cycling and, as

for water tests, was offset with respect to pressure. On the other hand, the density signals varied but without an appreciable period. The snapshots indicated that the fracture initiated at the early stage of fatigue and grew rapidly in the final cycle. The failure appeared to be axial fracture dominantly with secondary transverse fracture.

Fatigue responses in foam fracturing are summarized and presented in Fig. 10. Again, a higher fatigue rate, as defined above, was observed for the specimen with the shorter life. Also, the specimen with a higher initial injectivity tended to have a shorter fatigue lifetime.

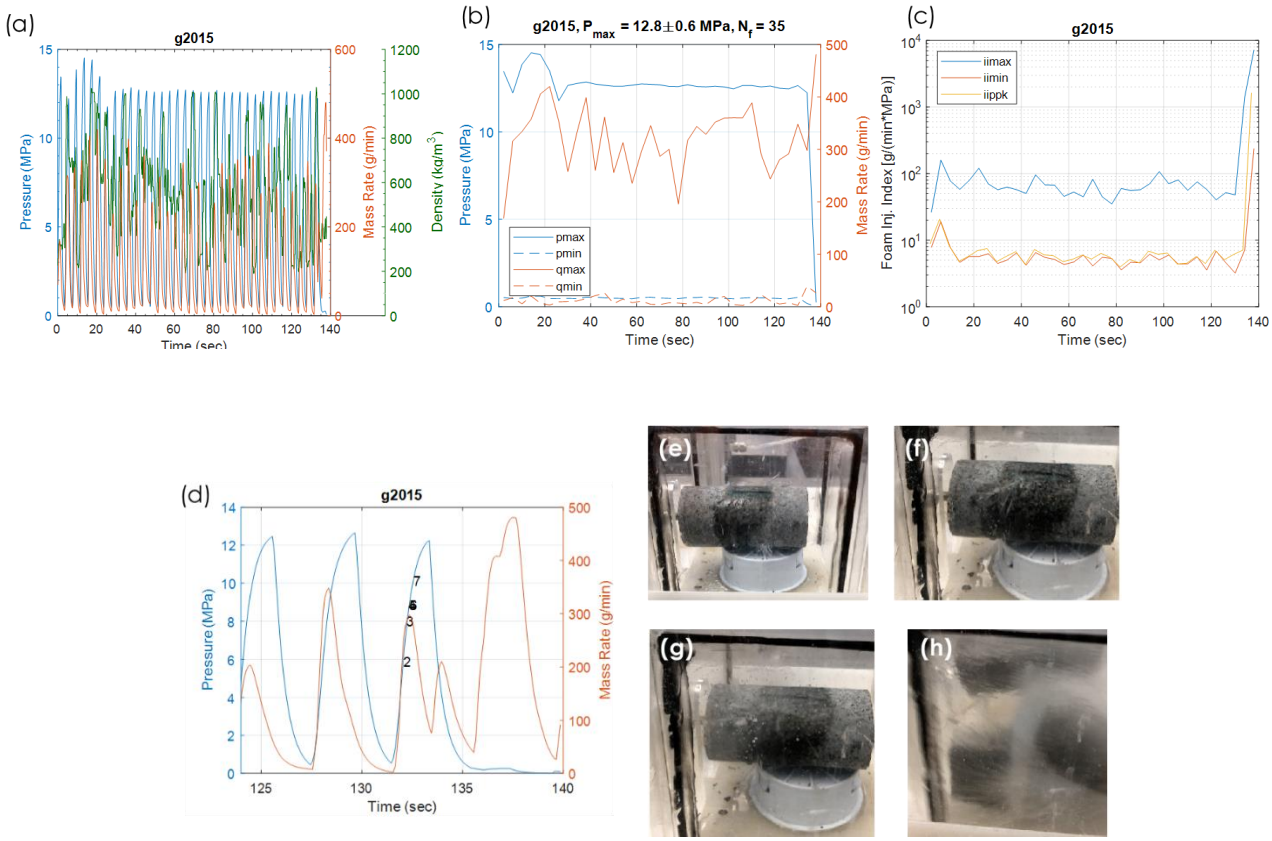

Figure 9: Cyclic injection responses of g2015, foam as a fracturing fluid: (a) pressure, mass rate and density, (b-c), maximum and minimum pressure, mass rate and injectivity index, (d) pressure and mass rate near failure cycle, (e) event 1: 28.95s fracture initiated with foam leaking, (f) 4: 132.36s mixture injection, (g) 5: 132.4s increased ejection, (h) 6: 132.45s breakup.

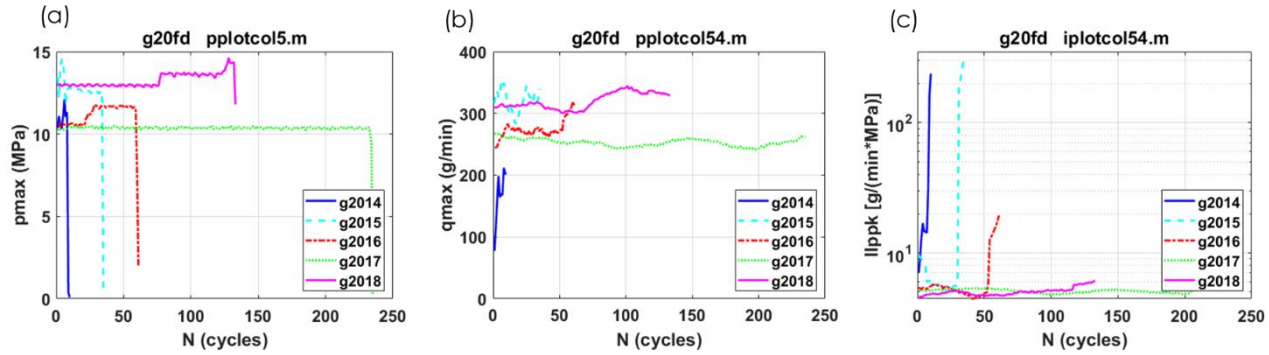

Figure 10: Cyclic injection responses for (a) maximum pressure, (b) mass flow rate; (c) injectivity index; foam as a fracturing fluid.

In general, experiments found that specimens can be fractured with a relatively small number of fatigue cycles (on the order of 100 cycles) as shown in Fig. 11. The fatigue pressure was approximately 75% of breakdown pressure obtained under monotonic injection for water fracturing and 60% of breakdown pressure for foam fracturing. This is important because it implies that the use of cyclic injection has the potential to reduce the breakdown pressure in an EGS system no matter if it is with water or foam as fracturing fluid. This reduced fracture pressure has added benefits of mitigating the risk of micro-seismicity related to reservoir stimulation and reduced stresses on pumping equipment.

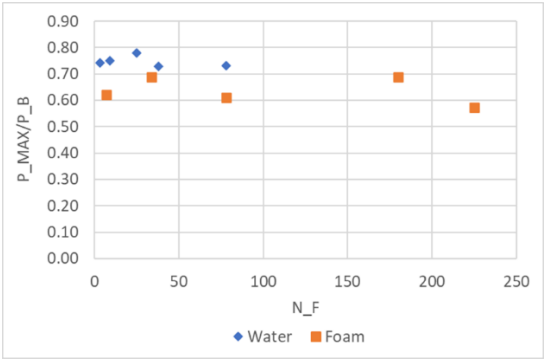

Figure 11: Ratio of maximum pressure in cycling to breakdown pressure in monotonic injection, P_MAX/P_B, as a function of number of cycles to failure, N_F. A 4-second period was used in the cyclic injection with 50% duty cycle.

4. DISCUSSION

4.1 Injectivity Index

Injectivity index (II) is a measure of the well fluid take at a given well head pressure or reservoir pressure. In this study, the II has been studied to characterize the injection response of materials under testing because pressure and flow rate are available from measurement and online monitoring.

For monotonic injection mode, the initially high II is associated with filling the test specimen section. The decline of II at the early stages of mass injection corresponds to the saturation of pressurization volume (Zhuang et al., 2019a). Following saturation of the test volume, the II is relatively constant for both water and foam injection until the initiation of breakdown. It is noted that the minimum II seen for water fracturing was less than the saturation level II prior to breakdown and is likely related to the pressurization configuration and relative incompressibility of water. The increasing II trend seen in Fig. 12 is likely due to subcritical fracture growth. Images from video footage of the experiments was used to measure the surface fracture size and orientation. Sub-critical fracture growth, as measured by length of the fracture in the axial direction, was generally corresponding to the II increase when water was the pressurization fluid. In the case of foam fracturing, the change in II was not significant while the breakdown occurred almost right after the fracture initiation with a short period of sub-critical growth. Note that the empty square marker in Fig. 12 (b) signifies the breakdown of each specimen. The abrupt II rise after that, in fact, corresponded to the post-failure stage.

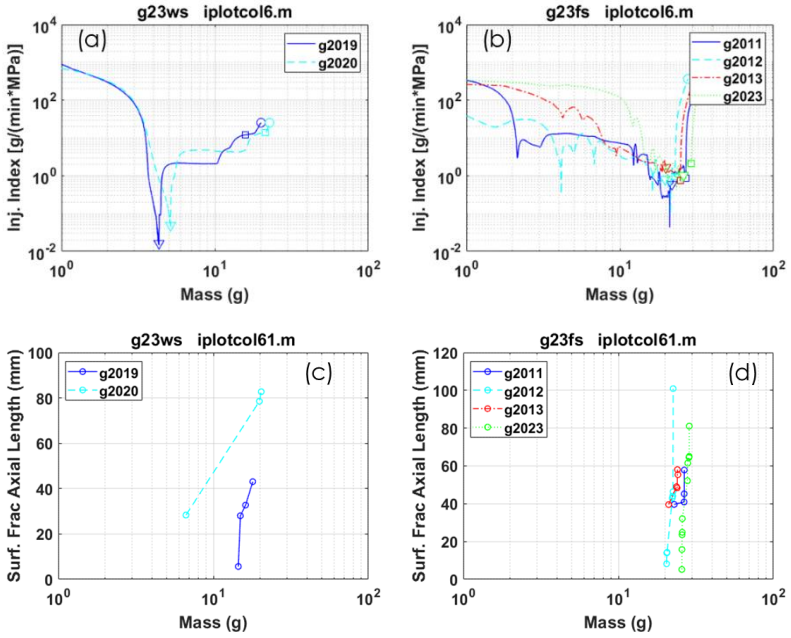

Figure 12: Responses as a function of injection mass: injectivity index for (a) water fracture and (b) foam fracturing; surface fracture size for (c) water fracturing and (d) foam fracturing.

For cyclic injection experiments, II evolution characterized the fatigue response well. We observed that faster II increase was related to a shorter fatigue life. Additionally, a higher initial II level corresponded to a faster II rise. Both observations imply a greater amount of initial structural damage within the test specimen. The degree of damage and damage evolution depended on the pressure amplitude of cycling as would be expected for a typical fatigue process.

4.2 Water Reduction and Replacement

The comparison of water consumption used for water and foam stimulation processes required filtering the density data for foam fracturing experiments to reduce the noise and spurious spikes in the data. The results of filtered density data for foam fracturing specimens under monotonic injection are shown in Fig. 13. Foam quality, as shown in Fig. 13(b) appeared to be consistent and stable during the injection process. The gas MRR as defined in Sect. 2.4, that measures the degree of potential water replacement, increased with the injection mass with limited fluctuation. The analysis demonstrated that the replacement of water in a foam fracturing can be more than 70% at the fracture initiation and at that level or higher after the fracture initiation.

The averages of critical threshold pressures and mass flow rates and pressures and cumulative mass injected are given in Fig. 14 with error bars describing the variation in experimental data. The term WinF represents the water mass contained within the foam while IN and BR correspond to data averages at fracture initiation and breakdown respectively. At the point of breakdown, it is seen that the water mass rate in foam fracturing can be at least one order of magnitude lower than that of water fracturing. This difference in water use has two components for this particular experimental configuration. First, a large amount of water has been replaced by the gas as defined by the quality ratio of the fluid. Second, we observed that the sub-critical growth occurred over a very short time period for foam fracturing, almost immediately following the fracturing initiation. This is largely due to the compressible nature of foamed fluids and their ability to continue to supply energy to extend fractures as the fluid expands. Water, by comparison, must continue to be injected to extend fractures because it is incompressible. At the point of breakdown, it is seen that the water mass in foam fracturing was 50% that of water fracturing.

Similar data processing was conducted for cyclic injection and results are given in Fig. 15. The density was relatively stable for a defined pressure amplitude, with the exception of test specimen g2016 where an increasing trend was observed. This increasing trend is mainly attributed to the increase in flow rate during cycling. The average quality of foam for cyclic injection experiments varied from 40 to 80%. The gas mass rate ratio for the maximum in cycle pressure is estimated to be around 30%. Foam density during cyclic injection was generally higher than during monotonic foam injection, and thus foam quality and gas MRR were lower. This was mainly due to the lower injection pressure levels used in cyclic injection.

In this study, foam was discharged during the depressurization stage of cyclic pressurization experiments. The effect of foam discharge and recycling on the final water use is beyond the scope of this study and remains to be investigated in the future. An additional strategy for increasing water replacement would be to explore other candidate foams like those using CO_2 or supercritical CO_2 as a gaseous phase whose density is much higher than N_2.

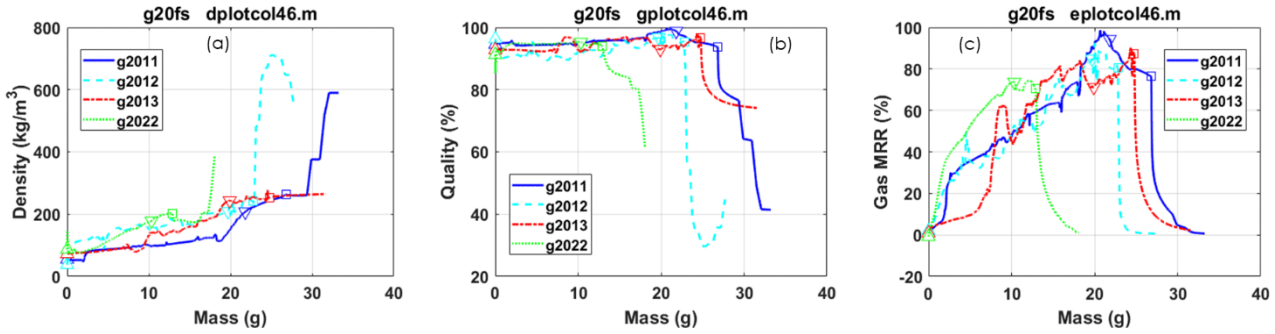

Figure 13: Foam response in terms of (a) density, (b) quality and (c) gas mass rate ratio (MRR).

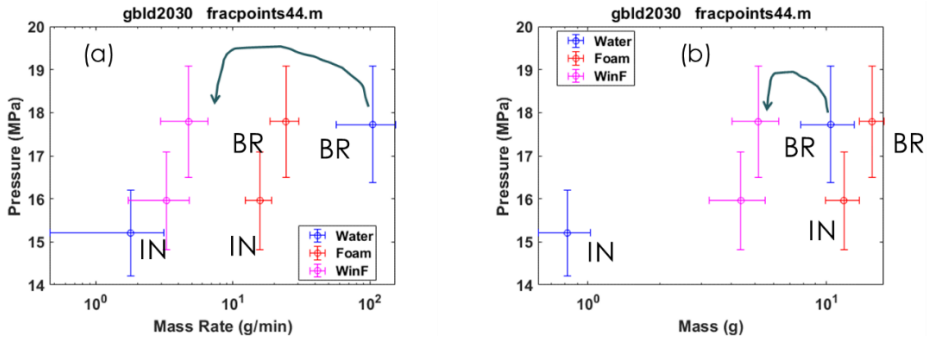

Figure 14: Fracture initiation and breakdown pressures as a function of (a) injection mass rate and (b) injection mass (amount related to cavity filling was removed).

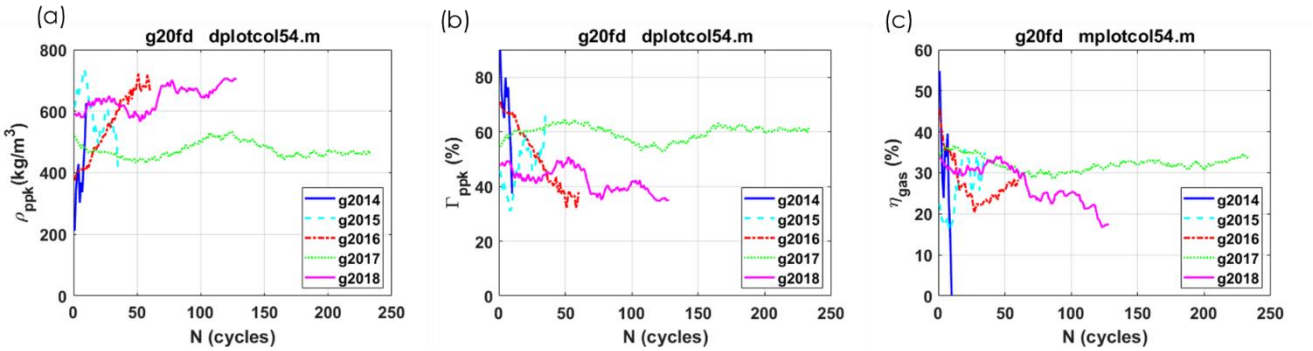

Figure 15: Cyclic injection responses for (a) density, (b) quality and (c) gas mass rate ratio; foam as a fracturing fluid.

4.3 Low Cycle Fatigue

Cyclic fatigue has been explored in cyclic stimulation in a couple of geothermal sites (Hofmann et al., 2019; Zang et al., 2019). The period of cycle varied from hours to seconds that were set up in the long, middle, and short terms of injection protocol with cyclic pressure lower than the breakdown pressure anticipated in conventional stimulation. The essence of cyclic stimulation lies in the use of depressurization to mitigate the risk of one-time energy release on micro seismicity involved with conventional stimulation. The repeated dynamic injection such as that used in this study serves the same purpose. It is noted that this approach is different from that of delayed initiation of fracture (Lu et al., 2015) or creep rupture in which the pre-determined creep load, lower than the breakdown strength obtained under monotonic loading, is applied to the materials to initiate breakdown by making use of time-related effects. In the delayed initiation of fracture approach, the release of stored energy is momentary and dynamic, whilst for cyclic injection, the release of stored energy is intermittent and controlled.

The results of cyclic injection are shown to be preferable to reservoir stimulation. It has been seen that a more connected fracture network can be created by using cyclic injection than that of monotonic injection (Zang et al., 2019; Zhuang et al., 2019b). A well-developed fracture network in reservoir can provide a high efficiency of heat exchange as required by EGS. In this study, we have observed fracture initiation, growth, and coalescence by using blind hole specimens. The experimental work described in this paper focused on specimen pressurization without confining pressure. The effect of confining pressure on the fracture initiation and development for the materials under foam fracturing remains to be studied.

While it makes use of cyclic fatigue to reduce the breakdown pressure with many benefits, cyclic injection may also bear some downsides. One of the concerns is the operation expense because the cyclic fatigue process can be longer than a monotonic injection process. As mentioned above, the major motivation to introduce the cyclic injection into hydraulic stimulation is to suppress the seismic energy. Therefore, the final adaption of cyclic injection in an EGS site is subjected to cost and risk analysis. The operational cost can be related to the pump energy or injection energy consumed in a fracturing job, E, which can be expressed as

$$E = \int p \cdot \dot{M} / \rho \cdot dt \,, \tag{9}$$

where p, $\dot{M}$, ρ have the meanings as specified in Sect. 2.4. A preliminary analysis of injection energy was conducted for water fracturing and the E was estimated to be 153 ± 61 J and 340 ± 269 J for monotonic and cyclic injections, respectively. The analysis has removed the amount of water mass used to fill cavities but not pressurize the specimen. Apparently, the energy consumption in the cyclic injection was higher than the monotonic injection, which is mainly because of a relatively high mass flow rate used in cycling. However, the pump energy data for hydraulic fracturing jobs are usually not available in the field. A numerical study, conducted by Zang et al. (2013), revealed that the accumulative seismicity energy can be reduced by 78% using cyclic injection with the pump energy increased only about 39%.

The injection scheme obviously needs to be optimized if the cyclic injection is recommended to control the seismicity in an EGS site. The waveform of cyclic injection and the injection parameters for a maximized reduction of breakdown pressure and a maximized use of fracturing fluids can be studied by using the laboratory setup in the future.

5. CONCLUSIONS

This paper described the composition and operating characteristics of an experimental monotonic or pulsed pressure foam injection system for fluid fracture testing of geological specimens in support of laboratory-scale EGS reservoir stimulation investigation. The system has a pressure rating of 6,000 psi (41.4 MPa) and has automated controls for injecting single phase or variable quality foam. Computer controlled flow control valves and a set of pressure regulators are used to cycle system maximum and minimum pressures values at user specified frequencies up to 50 Hz to enable the investigation of cyclic fatigue effects during hydraulic fracturing.

Experimental results were reported for water and foam fracturing tests performed on Charcoal Black granite without confining pressure. Cylindrical specimen geometries with a blind hole were studied using water and nitrogen-gas-in-water foam as the fracturing fluids. The effects of fracturing fluids and injection modes on the breakdown pressure and failure responses of the material were examined in detail.

Pressures at fracture initiation and breakdown were generally higher in foam fracturing than in water fracturing, but the average difference was less than 5%. For foam fracturing, it was observed that the breakdown occurred almost immediately following fracture initiation. For water fracturing, breakdown occurred over a significantly longer time period and was associated with sub-critical fracture growth following fracture initiation. At nominally the same level of breakdown pressure, the water mass used for foam fracturing experiments was approximately 50% of that the water mass used for water fracturing experiments.

A significant reduction in breakdown pressure required for fracture initiation and breakdown was also observed for cyclic injection in this study. For a comparable number of fatigue cycles, it was shown that 75% of the monotonic breakdown pressure could be used for water fracturing experiments and 60% of the monotonic breakdown pressure could be used for foam experiments, The number of fatigue cycles for the experimental set ranged from 4 to 225 cycles with an average of 68 cycles. The reduced operating pressure for initiating fracture has multiple potential field application benefits including reducing the risk associated with stimulation-induced micro-seismicity and reducing the burden on and reliability of surface equipment associated with higher pressure operation.

ACKNOWLEDGMENTS

This research was sponsored by the US Department of Energy, Assistant Secretary for Energy Efficiency and Renewable Energy, Geothermal Technologies Office, as part of the Enhanced Geothermal Systems Program under Contract No. DE-AC05-00OR22725 with the US Department of Energy.

Authors are grateful to David Wilson, Darren Loposser, Danny Parrott, Anthony McBee, Nathan Grundy, Cody West, Matt Rumbolt, James Oran, April Case, Eric Loyd of the ORNL for their help in flow control, line assembling, and pressure system evaluation; Harmon Phillips of Control Management Technology, Jason Reynolds of Intek, Carmen Bracco of TEK CV&F, Timothy Cavicchio of High Pressure Equipment, Eric Balcerzak & Will Hewitt of Swagelok, Larry Miller of Airgas, Marco Escobar of SC Hydraulic Engineering, Rao Choday of SFP for their help and discussion on fluid measurement and control. Authors also thank Drs. Lianshan Lin, James Hemrick, Edgar Lara-Curzio of ORNL for their review of this manuscript and comments.

REFERENCES

Chabora, E., Zemach, E.: Desert Peak EGS Project, Geothermal Technologies Program 2013 Peer Review, U.S. DOE EERE, Apr. 22, 2013.

Clark, C.E., Harto, C.B., Sullivan, J.L., Wang, M.Q.: Water Use in the Development and Operation of Geothermal Power Plants, ANL/EVS/R-10/5, Jan. 2011

Faroughi, S.A., Pruvot, A.J.-C.J., and McAndrew, J.: The Rheological Behavior of Energized Fluids and Foams with Application to Hydraulic Fracturing: Review, *J. of Petroleum Sci. and Eng.*, **163**, (2018), 243-263.

Freyman, M.: Hydraulic Fracture & Water Stress: Water Demand by the Numbers, Ceres, Feb. 2014.

Haimson, B., Fairhurst, C.: 1969, Hydraulic Fracturing in Porous-Permeable Materials. *J. of Petroleum Tech.*, July 1969: 811-817.

Hofmann, H., Zimmermann, G., Farkas, M., Huenges, E., Zang, A., Leonhardt, M., Kwiatek, G., Martinez-Garzon, P., Bohnhoff, M., Min, K.-B., Fokker, P., Westaway, R., Bethmann, F., Meier, P., Yoon, K. S., Choi, J. W., Lee, T. J., Kim K. Y.: First field application of cyclic soft stimulation at the Pohang Enhanced Geothermal System site in Korea, *Geophys. J. Int.*, **217**, (2019) 926–949.

Li, X., Feng, Z, Han, G., Elsworth, D., Marone, C., Saffer, D.: Hydraulic Fracturing in Shale with H_2O, CO_2 and N_2, The 49th US Rock Mechanics / Geomechanics Symposium, San Francisco, CA, USA, June 28-July 1, 2015, ARMA 15-786.

Lu, G., Uwaifo, E.C., Ames, B.C., Ufondu, A., Bunger, A.P., Prioul, R., and G. Aidagulov: Experimental Demonstration of Delayed Initiation of Hydraulic Fractures below Breakdown Pressure in Granite, The 49th US Rock Mechanics/ Geomechanics Symposium, San Francisco, California, June 28-July 1, 2015, ARMA 15-190.

Thakore, V., Ren, F., Voytek, J., Xi, J., Wang, H., Wang, J.-A. J., Polsky, Y.: High-Temperature Stability of Aqueous Foams as Potential Waterless Hydrofracking Media for Enhanced Geothermal Systems (EGS), *Proceedings*, 45th Workshop on Geothermal Reservoir Eng., Stanford U., Stanford, CA, Feb. 10-12, 2020, SGP-TR-216, 535-544.

Thakore, V., Ren, F., Voytek, J., Wang, H., Wang, J.-A. J., Polsky, Y.: High Temperature Stability of Aqueous Foams for Potential Application in Enhanced Geothermal System (EGS), *Proceedings*, 46th Workshop on Geothermal Reservoir Eng., Stanford U., Stanford, CA, Feb. 16-18, 2021, SGP-TR-218.

U.S. DOE: GeoVision, Harnessing the Heat Beneath Our Feet, 2019, https://www.energy.gov/eere/geothermal/downloads/geovision-harnessing-heat-beneath-our-feet, accessed Jan. 2020.

Valvias: Gas Density, www.valvias.com/miscellanea-material-properties-gases-density.php, accessed on 7/25/2020.

Wang, H., Wang, J.-A.J., Polsky, Y., Ren, F.: Research Considerations for Foam Fracturing in Stimulation Development for Enhanced Geothermal Systems, *Proceedings*, 44th Workshop Geotherm. Reservoir Eng., Stanford University, Stanford, CA, Feb. 11-13, 2019, SGP-TR-214, 617-627.

Wang, H., Wang, J.-A.J., Polsky, Y., Ren, F., Li, H., Thakore, V., Xi, J.: Study of Foam Fracturing for Enhanced Geothermal Systems Using Model Material, *Proceedings*, 45th Workshop on Geothermal Reservoir Engineering, Stanford University, Stanford, CA, Feb. 10-12, 2020, SGP-TR-216, 545-555.

Wanniarachchi, W.A.M., Ranjith, P.G., Perera, M.S.A., Rathnaweera, T.D., Zhang, D.C., Zhang, C.: Investigation of Effects of Fracturing Fluid on Hydraulic Fracturing and Fracture Permeability of Reservoir Rocks: An Experimental Study Using Water and Foam Fracturing, *Eng. Fract. Mech.*, **194**, (2018), 117-135.

Xie, L., Min, K.-B. & Song, Y.: Observations of Hydraulic Stimulations in Seven Enhanced Geothermal System Projects, *Renewable Energy*, **79**, (2015) 56-65.

Zang, A., Yoon, J.S., Stephansson, O., Heidbach, O.: Fatigue Hydraulic Fracturing by Cyclic Reservoir Treatment Enhances Permeability and Reduces Induced Seismicity, *Geophys. J. Int.*, **195**, (2013), 1282-1287.

Zang, A., Zimmermann, G., Hofmann, H., Stephansson, O., Min, K.-B. Kim, K. Y.: How to Reduce Fluid-Injection-Induced Seismicity, *Rock Mech. and Rock Eng.*, **52**, (2019) 475–493.

Zhuang, L., Kim, K.Y., Jung, S.G., Diaz, M., and Min, K.-B.: Effect of Water Infiltration, Injection Rate and Anisotropy on Hydraulic Fracturing Behavior of Granite, *Rock Mech Rock Eng.*, **52**, (2019a), 575–589.

Zhuang, L., Kim, K.Y., Jung, S.G., Diaz, M., Min, K.-B., Zang, A., Stephansson, O., Zimmermann, G., Yoon, J.-S., & Hofmann, H.: Cyclic Hydraulic Fracturing of Pocheon Granite Cores and Its Impact on Breakdown Pressure, Acoustic Emission Amplitudes and Injectivity, *Int. J. of Rock Mech. and Min. Sci.*, **122**, (2019b), 104065.

Zimmermann, G., Moeck, I., Blöcher, G.: Cyclic Waterfrac Stimulation to Develop an Enhanced Geothermal System (EGS) - Conceptual Design and Experimental Results, *Geothermics*, **39**, (2010) 59–69.